Shinmoto and Baba
Progress in Earth and Planetary Science (2024) 11:50
https://doi.org/10.1186/s40645-024-00647-6

Progress in Earth and Planetary Science

RESEARCH ARTICLE Open Access

A methodology for appropriate withdrawal of tsunami warnings based on numerical simulations

Naoko Shinmoto[1] and Toshitaka Baba[2*]

Abstract

This study performed large-scale numerical simulations for predicting the attenuation of tsunamis caused by the 2011 Tohoku, Japan, and 2010 Maule, Chile earthquakes, recorded at Japanese tide gauges. Tsunami amplitude waveforms were generated by computing the moving root-mean-square of the data for quantitative analyses. Sensitivity analysis showed that tsunami nonlinearity and computational grid intervals near the tide gauges significantly impact the prediction of tsunami attenuation. The predicted withdrawal times of tsunami warnings agreed with the observations; however, time discrepancies were observed for advisory withdrawals at several stations. Using the proposed method, we predicted the warning period of a great interplate earthquake in the Nankai Trough to be approximately one day. These findings can provide critical information for disaster prevention because the withdrawal of warnings is directly related to permission to enter coastal areas affected by the tsunami, whereas unnecessarily long warnings hinder rescue operations.

1 Introduction

Tsunami disaster mitigation requires an understanding of the generation, propagation, and attenuation processes of tsunamis. Understanding tsunami generation and propagation enables the prediction of tsunami arrival times and their heights. The withdrawal of tsunami warnings is directly related to the attenuation process. According to the Japan Meteorological Agency (JMA) (2006) and Koshimura et al. (2007), the maximum tsunami due to the 2006 Kuril earthquake occurred after the withdrawal of tsunami warnings in many locations along the Japanese coast. Inappropriate withdrawal may cause severe damage because the movement of people resumes in coastal areas after the withdrawal of tsunami warnings. However, unnecessary long tsunami warnings should be avoided because their withdrawal signals the end of the tsunami threat and the beginning of full-scale rescue operations, sheltering, and other recovery activities. Prolonged evacuation under a tsunami warning can cause significant stress to the residents. Timely withdrawal will reduce this psychological burden and bring mental stability. Additionally, economic activities in coastal areas are suspended during a tsunami warning, and prolonged warnings exacerbate the economic impact. Proper withdrawal of warnings helps maintain residents' confidence in public disaster information, resulting in prompt and appropriate evacuation actions in future disasters. Therefore, accurately predicting the tsunami attenuation process is crucial.

Hayashi et al. (2010) defined the moving root-mean-square (MRMS) amplitude of tsunami waveforms for performing a quantitative analysis of tsunami attenuation. Using MRMS amplitude waveforms, Hayashi et al. (2010)

*Correspondence:
Toshitaka Baba
baba.toshi@tokushima-u.ac.jp
[1] Graduate School for Sciences and Technology for Innovation, Tokushima University, Tokushima, Japan
[2] Graduate School for Social and Industrial Science and Technology, Tokushima University, 2-1 Minami-jyosanjima-cho, Tokushima 770-8506, Japan

analyzed the tsunamis of the 2006 and 2007 Kuril earthquakes, which stuck on the Japanese coast. The MRMS amplitude waveforms in the decay process recorded by tide gauges were approximated by an exponential function, with the time constant of decay determined using regression analysis. JMA (2021) attempted to predict tsunami attenuation by fitting an approximate curve to the MRMS amplitudes of the observed waveforms. Saito et al. (2013) used numerical tsunami simulations and adjusted coefficients of bottom friction terms to reproduce the tsunami attenuation recorded at ocean bottom pressure gauges for the 2011 Tohoku earthquake. Davies et al. (2020) also demonstrated the importance of bottom friction terms using distant tsunamis that were observed in Australia. Imai et al. (2014) found that the attenuation in coastal areas was slower than that in offshore areas. Tanioka et al. (2019) highlighted the effect of seiche on long-lasting tsunamis in a bay.

Despite the above-mentioned efforts, the tsunami attenuation processes remain unclear. Currently, tsunami warnings are withdrawn based on empirical judgments and real-time tsunami monitoring. The empirical method by JMA (2021) can be used to predict tsunami attenuation quantitatively; however, this method can only be applied after tsunami decay starts. Therefore, in this study, we developed an alternative method based on large-scale tsunami simulations to predict the attenuation of the tsunami MRMS amplitudes. Using this method, we reproduced the attenuation of the tsunami MRMS amplitudes recorded at Japanese tide gauges for the 2011 Tohoku, Japan, and 2010 Maule, Chile earthquakes (Fig. 1). The March 11, 2011, Tohoku earthquake, which was an interplate earthquake, occurred in the Japan Trench at a depth of 24 km with a moment magnitude (Mw) of 9.0. The earthquake generated tsunamis with a height of more than 9.3 m as recorded at a tide gauge in Soma City (JMA 2011) and with a maximum run-up of approximately 40 m as measured by post-earthquake surveys (Mori et al. 2012). The February 27, 2010, Maule earthquake, which was also an interplate earthquake, occurred in the Chile Trench, at a depth of 20 km with Mw 8.8 (JMA 2010a). The earthquake generated a tsunami that reached the coast of Japan approximately 23 h later. A tsunami of 1.2 m height was recorded at a port in Japan (JMA 2010b).

We performed sensitivity tests by varying the calculation conditions to understand the key factors that affect the attenuation process. Simulation-based withdrawals of tsunami warnings and advisories were compared with those by the observed waveforms. Finally, we predicted the withdrawal times of tsunami warnings and advisories for a potential future earthquake that can occur in the Nankai Trough.

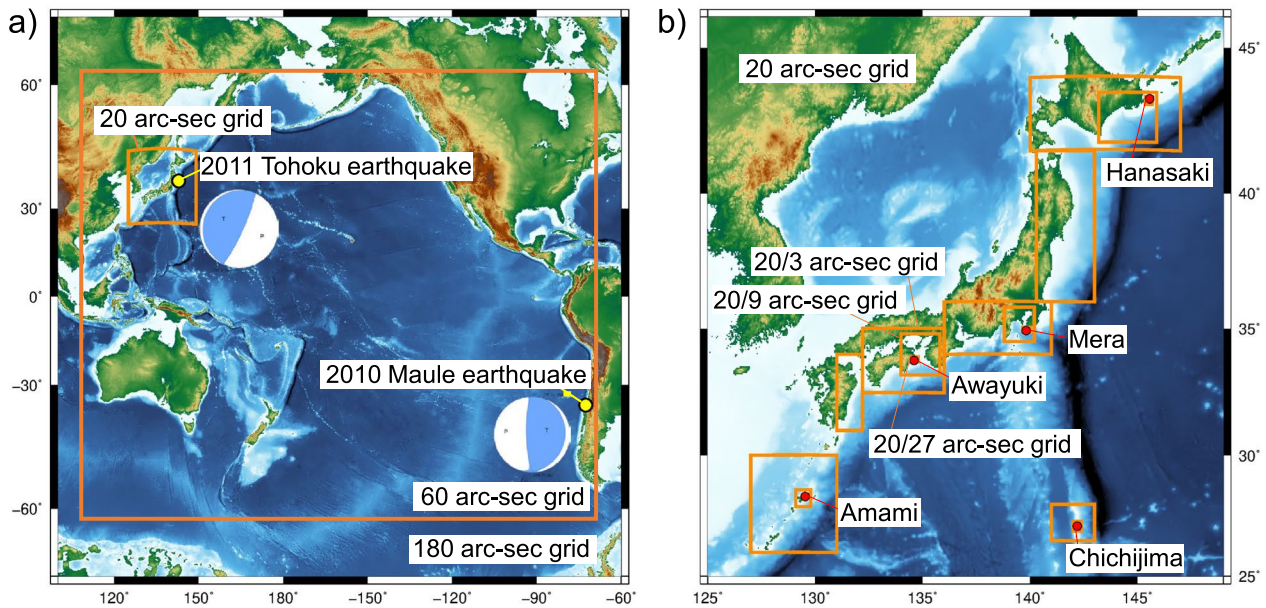

Fig. 1 The nested grid system used for tsunami simulation. **a** The whole computational area. Yellow dots indicate the epicenters of the earthquakes. Moment tensor solutions were obtained from the U.S. Geological Survey catalog. **b** The area around Japan showing the locations of tide stations (red dots) used in this study

2 Data and methods

We acquired tsunami waveforms of the 2011 Tohoku and 2010 Chile earthquakes recorded by JMA tide gauges with the data sampling interval of 15 s (Fig. 1). The tidal components were removed from the original data to retrieve tsunami waveforms using the tide prediction software NAOTIDEJ (Matsumoto et al. 2000) and applying a 3-h high-pass filter using the seismic analysis code (George et al. 2013). We generated tsunami MRMS waveforms using the method described by Hayashi et al. (2010), which considered a moving average with a time width of 64 min on the squared root of the tsunami waveforms. The background amplitude of the MRMS waveform calculated from data for the 3 h before the tsunami arrival was subtracted from the entire tsunami MRMS waveform to remove background noise.

For tsunami simulations, we solved the linear (Eqs. 1–3) and nonlinear (Eqs. 4–6) long-wave equations as follows:

$$\frac{\partial Hu}{\partial t} = -\frac{gH}{R\sin\theta}\frac{\partial \eta}{\partial \varphi} - fHv \tag{1}$$

$$\frac{\partial Hv}{\partial t} = -\frac{gH}{R}\frac{\partial \eta}{\partial \theta} + fHu \tag{2}$$

$$\frac{\partial \eta}{\partial t} = -\frac{1}{R\sin\theta}\left(\frac{\partial Hu}{\partial \varphi} + \frac{\partial Hv\sin\theta}{\partial \theta}\right) \tag{3}$$

$$\frac{\partial M}{\partial t} + \frac{1}{R\sin\theta}\frac{\partial}{\partial \varphi}\left(\frac{M^2}{H+\eta}\right) + \frac{1}{R}\frac{\partial}{\partial \theta}\left(\frac{MN}{H+\eta}\right) = -\frac{g(H+\eta)}{R\sin\theta}\frac{\partial \eta}{\partial \varphi} - fN - \frac{gn^2}{(H+\eta)^{7/3}}M\sqrt{M^2+N^2} \tag{4}$$

$$\frac{\partial N}{\partial t} + \frac{1}{R\sin\theta}\frac{\partial}{\partial \varphi}\left(\frac{MN}{H+\eta}\right) + \frac{1}{R}\frac{\partial}{\partial \theta}\left(\frac{N^2}{H+\eta}\right) = -\frac{g(H+\eta)}{R}\frac{\partial \eta}{\partial \theta} + fM - \frac{gn^2}{(H+\eta)^{7/3}}N\sqrt{M^2+N^2} \tag{5}$$

$$\frac{\partial \eta}{\partial t} = -\frac{1}{R\sin\theta}\left(\frac{\partial M}{\partial \varphi} + \frac{\partial N\sin\theta}{\partial \theta}\right) \tag{6}$$

where u and v are the corresponding horizontal flow velocities along the longitude (φ) and co-latitude (θ) directions, η is the water level, H is the depth of the ocean at rest, t is the time, R is the Earth's radius, g is the gravitational acceleration, f is the Coriolis parameter and n is Manning's roughness coefficient. M and N are the depth-integrated flow quantities equal to $(H+\eta)v$ and $(H+\eta)u$, respectively. The linear tsunami model did not include tsunami inundation on land, resulting in perfect reflection at the boundary between land and sea. In the nonlinear tsunami model, a moving boundary algorithm was used to simulate tsunami inundation on land when the water level rose above the coastal elevation.

We conducted tsunami simulations using the open-source tsunami software JAGURS (Baba et al. 2015, 2017), which is a finite-difference code of the leapfrog, staggered grid with nested domains. We used bathymetric datasets consisting of nested domains at six levels (Fig. 1b) with the grid intervals of 180, 60, 20, 20/3, 20/9, and 20/27 arc sec (approximately 23 m along the latitude, 17–20 m along longitude directions), respectively. Gridded bathymetry data were constructed using a combination of ETOPO1 (Amante and Eakins 2009), the Global Tsunami Terrain Model (GtTM, Chikasada 2020), and digital elevation models gridded at 5-m and 10-m intervals by the Geospatial Information Authority of Japan (see Availability of data and materials). We simulated the coarsest domain gridded at 180 arc sec using the linear long-wave equations to stabilize the computation. We applied an open boundary condition that assumed that tsunami propagated with phase velocity of $\sqrt{gH}$ at the outer edges of the coarsest domain. For the remaining domains, we switched between the linear and nonlinear equations, as shown in Table 1, to investigate the effects of tsunami nonlinearity and grid intervals on tsunami attenuation predictions. We used constant bottom friction coefficient ($n = 0.025$) in the nonlinear computation domains.

For the tsunami sources, we used the fault models derived from tsunami inversion analyses (Satake et al. 2013; Yoshimoto et al. 2016) and an analytic solution

Table 1 Descriptions for tsunami propagation models

	Model 1	Model 2	Model 3	Model 4	Model 5
180 arc-sec grid	Linear	Linear	Linear	Linear	Linear
60 arc-sec grid	Linear	Nonlinear	Nonlinear	Nonlinear	Nonlinear
20 arc-sec grid	Nonlinear	NonLinear	NonLinear	Nonlinear	Nonlinear
20/3 arc-sec grid	Not used	Not used	NonLinear	Nonlinear	Nonlinear
20/9 arc-sec grid	Not used	Not used	Not used	Nonlinear	Nonlinear
20/27 arc-sec grid	Not used	Not used	Not used	Not used	Nonlinear

to calculate crustal deformation due to fault motion (Okada 1985). We also included the additional tsunami generation by the horizontal movement of the seafloor slope (Tanioka and Satake 1996). A hydraulic filter proposed by Kajiura (1963) was applied to the calculated vertical deformation to account for the non-hydrostatic effect of fluids in tsunami generation. The time step width was at 0.1 s to satisfy the computational stability condition in the tsunami simulation. The model was integrated for 60 and 80 h for the 2011 Tohoku and 2010 Maule earthquakes, respectively. Simulations were performed on the FUJITSU Supercomputer PRIMEHPC FX1000 at the Information Technology Center, at the University of Tokyo.

3 Simulation results

The nonlinearity of tsunamis is significant in shallow coastal areas; therefore, we inevitably used the nonlinear long-wave equations on the domains with grid intervals smaller than 20 arc sec. Previous studies suggested that bottom friction in the Pacific Ocean could affect tsunami attenuation (Saito et al. 2013; Davies et al. 2020). Therefore, we calculated tsunami propagation in the domain of 60 arc-sec grid intervals by solving the linear (Model 1) and nonlinear long-wave equations (Model 2, see Table 1). In Model 1, numerical instabilities occurred at the coastline in the domain of the 60 arc-sec grid interval after 48 and 72 h for the 2011 Tohoku and 2010 Maule earthquakes, respectively. Unfortunately, the reason for the numerical instability is unclear. Since wave energy does not decay in the linear model, numerical errors might have accumulated during the long calculations.

In the 2011 Tohoku tsunami simulations, the presence (red in Fig. 2a) or absence (blue) of nonlinearity did not have a significant effect on MRMS amplitude immediately after the earthquake. However, the differences in the MRMS amplitudes became significant approximately 24 h after the earthquake. In the linear long-wave calculations, the attenuation of the MRMS amplitude waveforms was weak. At 24 h, the tsunami waves reflected from the North American continent reached the coast of Japan. Because bottom friction is significant in shallow waters, we speculated on energy dissipation in shallow waters off the North American coast. Although nonlinear effects were included in Model 2 in all the domains, the MRMS amplitudes of the simulated waveforms remained larger than those of the observed at Awayuki and Chichijima tide gauge stations. Conversely, the MRMS amplitude of the simulated waveforms was smaller than that of the observed during the first 20 h at Amami.

Figure 2b shows the MRMS amplitude waveforms for the 2010 Maule earthquake. In this case, in contrast to the 2011 Tohoku earthquake, the MRMS amplitudes of Models 1 and 2 differed immediately after the arrival of the tsunami at the gauge stations around Japan. As the 2010 Maule earthquake was a far-field one, the first wave was followed by tsunamis that propagated via various paths, including reflections on the Chilean coast where the nonlinear effect was significant. At Hanasaki, Mera, and Awayuki, the MRMS amplitude waveforms of Model 2 were not in agreement with those of the observed waveforms, similar to the case of the 2011 Tohoku earthquake.

Next, we used fine-grid intervals with a nested algorithm (Models 3–5 in Table 1, Fig. 3a) for the 2011 Tohoku earthquake, which improved the agreement between simulations and observations at Chichijima and Awayuki. For the 2010 Maule earthquake (Fig. 3b), the effects of the fine-grid intervals were less apparent than those of the 2011 Tohoku earthquake. However, the normalized root-mean-square errors improved slightly for Awayuki. Based on these results, we conclude that the nonlinear long-wave equations and fine-grid intervals near tide stations are necessary to predict MRMS amplitude waveforms. However, it is challenging to determine the appropriate grid intervals because the characteristic wavelengths of the topography near the tide stations play a key role.

4 Discussion

4.1 Predicted and observed withdrawal times

Hayashi et al. (2010) compared the original waveforms of the tsunamis with its MRMS amplitude waveforms and found that the peak values of the original waveforms were always less than three times those of the MRMS amplitudes. Based on this relationship, we set the withdrawal time of tsunami warnings to be when the MRMS amplitude was consistently below 25.0 cm. The withdrawal time of tsunami advisories was set to be when the MRMS amplitude was below 8.3 cm. We compared the observed withdrawal times of warnings and advisories with those estimated using the MRMS amplitude waveforms (Fig. 4). For tsunami warnings, the standard deviation of the difference between the calculated using Model 5 (Table 1) and observed withdrawal times was estimated to be 4.5 h. The error was approximately 12 h when using a prediction method in previous studies (e.g., JMA 2021). Thus, our method can predict more accurately than previous studies.

For the 2010 Maule earthquake, the calculated withdrawals of advisories were inconsistent with the observations at Hanasaki and Amami. The standard deviation was estimated to be 14.1 h, which was much higher than that of the warnings. For the 2011 Tohoku earthquake, the MRMS amplitudes did not fall below 8.3 cm even 60 h after the earthquake at Hanasaki, Mera, and Chichijima; therefore, we could not predict the withdrawal times. Although we can adjust the decay curves empirically by

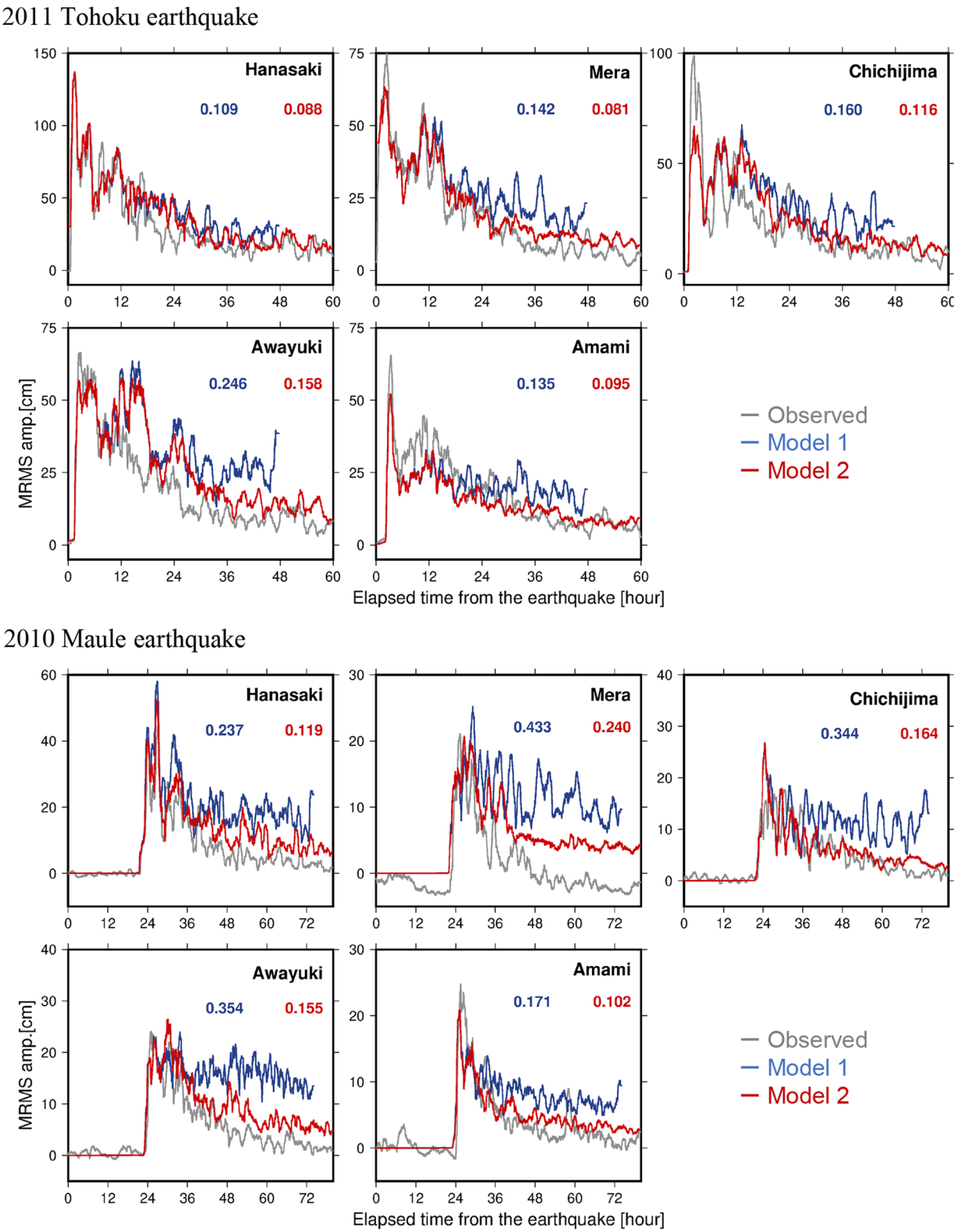

Fig. 2 Comparisons between moving root-mean-square (MRMS) amplitude waveforms computed using the observation (gray), Model 1 (blue), and Model 2 (red). **a** MRMS amplitude waveforms for the 2011 Tohoku earthquake and **b** MRMS amplitude waveforms for the 2010 Maule earthquake. The values in figures are the normalized root-mean-square errors between the observed and calculated MRMS amplitude waveforms. The MRMS amplitude waveforms for Model 1 are truncated at 48 (**a**) and 72 (**b**) hours due to numerical instabilities

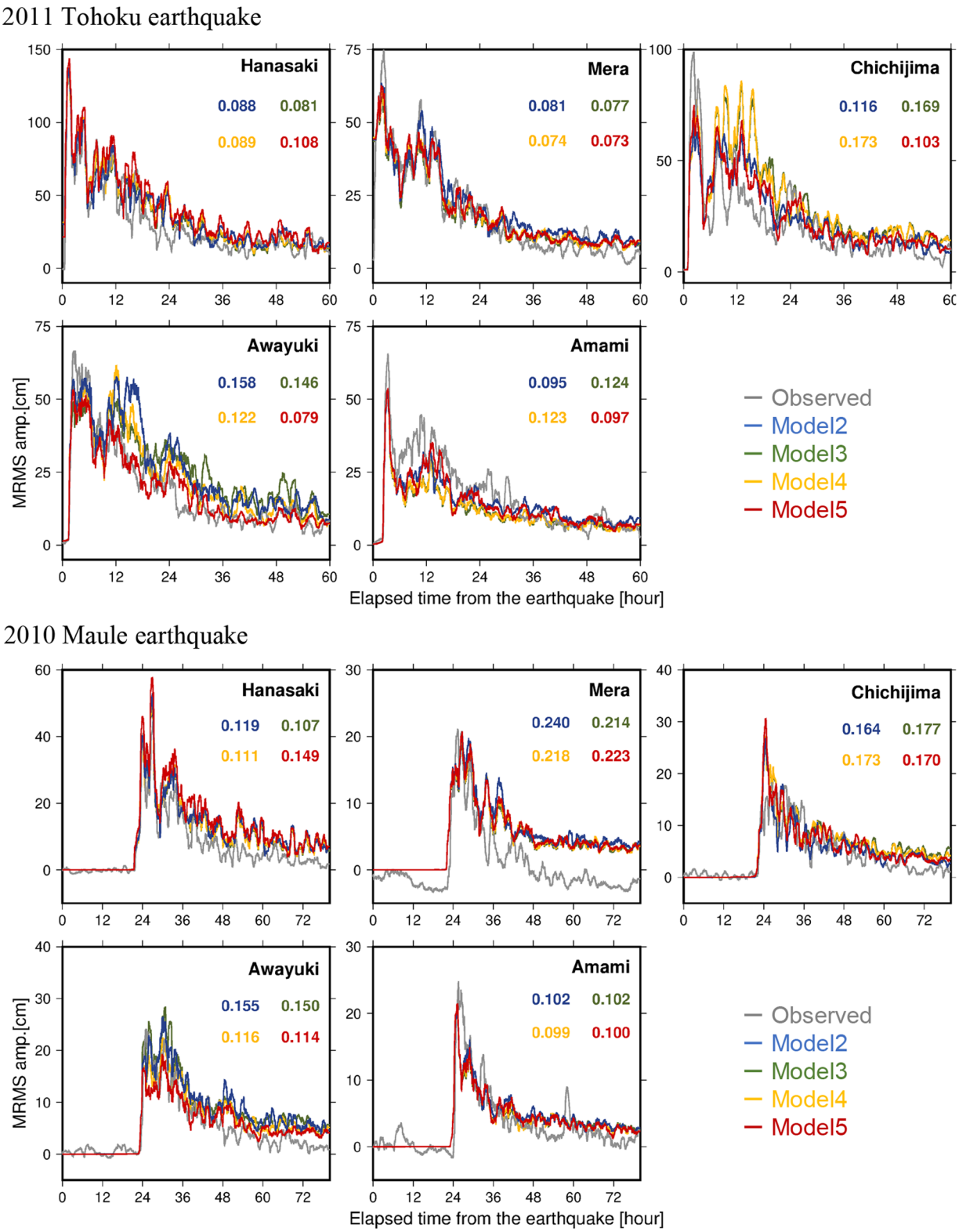

Fig. 3 Comparisons between moving root-mean-square (MRMS) amplitude waveforms obtained using the observation (gray) and Model 2–5. **a** MRMS amplitude waveforms for the 2011 Tohoku earthquake and **b** MRMS amplitude waveforms for the 2010 Maule earthquake. The values in figures are the normalized root-mean-square errors between the observed and calculated MRMS

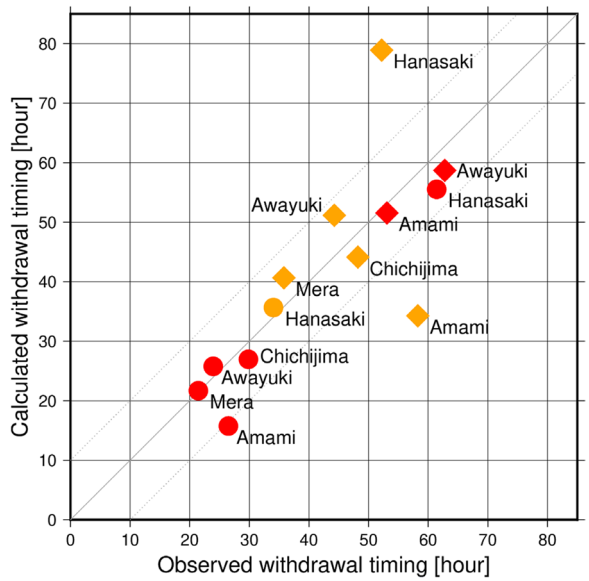

Fig. 4 Observed and calculated withdrawal times of tsunami warnings and advisories. Red and yellow circles represent the tsunami warnings for the 2011 Tohoku and 2010 Maule earthquakes, respectively. Red and yellow squares represent the tsunami advisories for the 2011 Tohoku and 2010 Maule earthquakes, respectively

changing the coefficients in friction terms, the physical mechanism of changing the coefficients should be scientifically understood. In addition, because the accuracy of the tsunami warning withdrawal was good, adjusting the coefficient would be challenging.

4.2 Withdrawal times of tsunami warnings caused by a great earthquake in the Nankai Trough

Interplate earthquakes occur repeatedly in the Nankai Trough, where the Philippine Sea Plate is subducting beneath the Eurasian Plate. The recurrence intervals of the earthquakes were estimated to be approximately 100–150 years, and almost 80 years have passed since the most recent earthquake in 1946. Therefore, we anticipate an earthquake accompanied by strong seismic shaking and a giant tsunami. The Cabinet Office (2012) has predicted tsunamis of up to 34 m in height on the southwestern coast of Japan. Consequently, tsunami warnings and advisories will be issued for an extended period. Therefore, we predicted the withdrawal timing of tsunami warnings and advisories in the event of an earthquake in the Nankai Trough. For the tsunami simulation, we used the fault

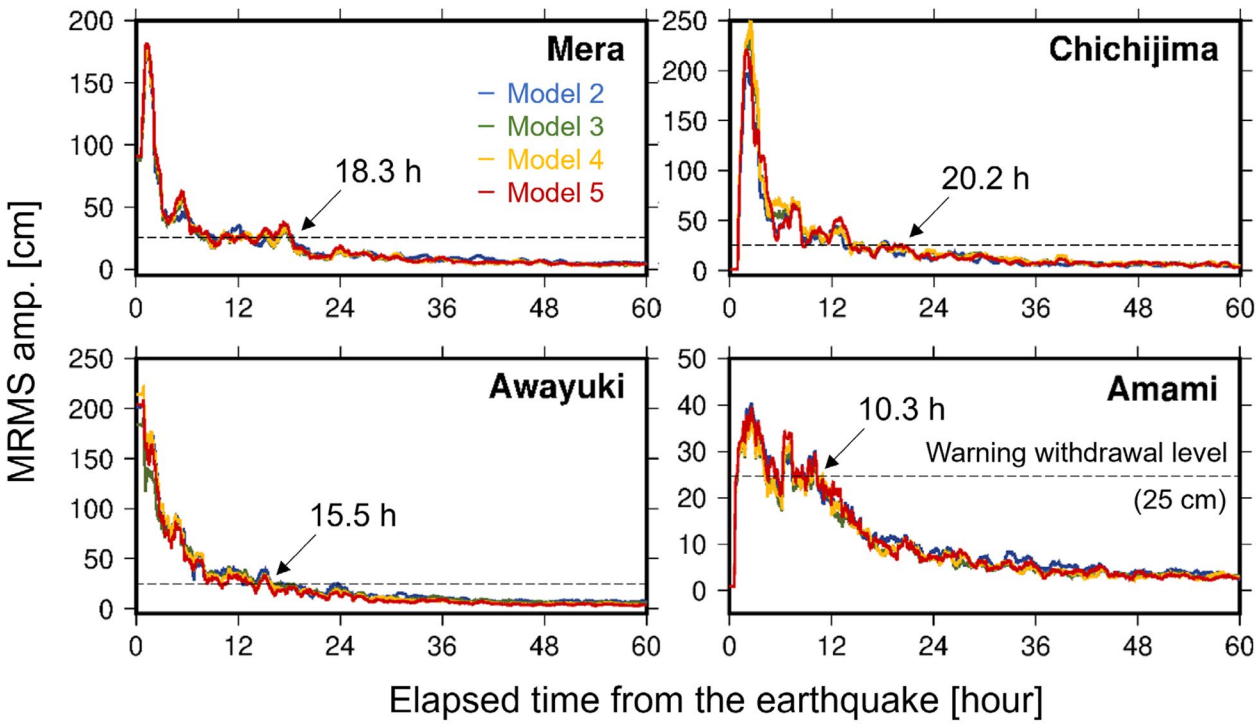

Fig. 5 Calculated moving root-mean-square (MRMS) amplitude waveforms using a fault model of the 1707 Hoei earthquake proposed by Furumura et al. (2011). The waveforms of Model 2–5 (Table 1) are shown. Dashed line indicates a threshold to withdraw the tsunami warnings. The tsunami warnings periods were estimated to be 18.3, 15.5, 20.2, and 10.3 h at Mera, Awayuki, Chichijima and Amami, respectively

model proposed by Furumura et al. (2011), which was used to simulate the tsunami caused by the 1707 Hoei earthquake, the most devastating earthquake in the Nankai Trough. We chose the MRMS amplitudes estimated using Model 5, based on the sensitivity analysis results. Hanasaki was excluded from the analysis because its energy attenuation was too low to calculate the advisory time.

Based on the MRMS amplitude waveforms, the tsunami warnings periods were estimated to be 18.3, 15.5, 10.3, and 20.2 h at Mera, Awayuki, Amami, and Chichijima, respectively (Fig. 5). The tsunami advisory periods ranged from 36.3 to 48.9 h. Considering the prediction errors, it was predicted that tsunami warnings would last for approximately one day and advisories would last from 2 to 2.5 days on the Japanese coast for a great earthquake in the Nankai Trough.

5 Conclusion

This study conducted large-scale tsunami simulations to identify tsunami calculation models that can simulate tsunami attenuation in coastal areas. We found that the simulation-based methods could predict the withdrawal times of tsunami warnings and advisories. Further, we investigated the effects of nonlinearity and computational grid intervals on tsunami simulations. The conclusions of this study are as follows.

1. Numerical simulations using the nonlinear long-wave equations with nested grids were successfully performed for 60 and 80 h for the tsunamis caused by the 2011 Tohoku and 2010 Maule earthquakes, respectively.
2. The effect of nonlinearity was significant in the prediction of tsunami attenuation.
3. Our simulation-based method predicted the tsunami warning withdrawal time with a standard deviation error of 4.5 h, but the accuracy of the advisory withdrawal was not as good as that of the warning.

For tsunami advisories, the prediction errors were large at Amami and Hanasaki. In this study, the effects of other parameters, such as horizontal eddy viscosity and dispersion, which may play essential roles in the tsunami attenuation process, were not investigated. In future research, we will incorporate these parameters and continue developing a long-term tsunami simulation model.

Acknowledgements
We appreciate considerate comments of anonymous reviewers and the handling editor, Dr. Takuto Maeda. These comments were very helpful in improving the manuscript. For our tsunami calculations, we used the FUJITSU Supercomputer PRIMEHPC FX1000 and the FUJITSU Server PRIMERGY GX2570 (Wisteria/BDEC-01) at the Information Technology Center, the University of Tokyo. The Japan Meteorological Agency provided tide-level observation records from tide stations.

Author contributions
N.S. performed the tsunami simulations and wrote the draft of the manuscript. T.B. managed the entire study and wrote the manuscript.

Funding
This work was supported by KAKENHI grants-in-aid from the Japan Society for the Promotion of Science [grant numbers JP22H01308, JP22H01742 and JP22H01750] and by the Earthquake Research Institute of the University of Tokyo [ERI JURP 2023-S-B101].

Availability of data and materials
We used the tsunami software JAGURS (Baba et al. 2015, 2017) provided in an online repository at https://doi.org/10.5281/zenodo.3737816. Tidal level observation data at 15-s sampling (tsunami) were obtained from the Japan Meteorological Business Support Center at http://www.jmbsc.or.jp/en/index-e.html. GtTM (Chikasada 2020) is available at https://kiyuu.bosai.go.jp/GtTM/. Digital elevation models gridded at 5 m and 10 m intervals by the Geospatial Information Authority of Japan are available at https://www.gsi.go.jp/kiban. The tide prediction model NAOTIDEJ (Matsumoto et al. 2000) is available at https://www.miz.nao.ac.jp/staffs/nao99/index_En.html.

Declarations

Competing interests
The authors declare that they have no competing interests.

Received: 11 March 2024 Accepted: 25 July 2024
Published online: 06 September 2024

References

Amante C, Eakins BW (2009) ETOPO1 1 Arc-minute global relief model: procedures, data sources and analysis. NOAA Technical Memorandum NESDIS NGDC-24. National Geophysical Data Center, NOAA. https://doi.org/10.7289/V5C8276M

Baba T, Takahashi N, Kaneda Y, Ando K, Matsuoka D, Kato T (2015) Parallel implementation of dispersive tsunami wave modeling with a nesting algorithm for the 2011 Tohoku Tsunami. Pure Appl Geophys 172:3455–3472. https://doi.org/10.1007/s00024-015-1049-2

Baba T, Allgeyer S, Hossen J, Cummins PR, Tsushima H, Imai K et al (2017) Accurate numerical simulation of the far-field tsunami caused by the 2011 Tohoku earthquake, including the effects of Boussinesq dispersion, seawater density stratification, elastic loading, and gravitational potential change. Ocean Model 111:46–54. https://doi.org/10.1016/j.ocemod.2017.01.002

Chikasada N (2020) Global Tsunami Terrain Model. https://kiyuu.bosai.go.jp/GtTM/. https://doi.org/10.17598/NIED.0021

Davies G, Romano F, Lorito S (2020) Global Dissipation models for simulating tsunamis at far-field coasts up to 60 hours post-earthquake: multi-site tests in Australia. Front Earth Sci 8:598235. https://doi.org/10.3389/feart.2020.598235

Furumura T, Imai K, Maeda T (2011) A revised tsunami source model for the 1707 Hoei earthquake and simulation of tsunami inundation of Ryujin Lake, Kyushu. Japan J Geophys Res 116:B02308. https://doi.org/10.1029/2010JB007918

George H, James W, Ian B (2013) The seismic analysis code A primer and user's guide. Cambridge University Press, Cambridge. https://doi.org/10.1017/CBO9781139547260

Hayashi Y, Imamura F, Koshimura S (2010) Feasibility of using decay characteristics on trends and fluctuations of Tsunami for forecasting Far-field Tsunami. J Japan Soc Civ Eng, Ser B2 66(1):I211–I215

Imai K, Tanobe A, Hayashi Y, Imamura F (2014) Decay process of the Tsunami due to the 2011 Great off the Pacific Coast of Tohoku earthquake along the Pacific Coast of Japan. J Japan Soc Civ Eng Ser B2 70(2):I276–I280

Japan Meteorological Agency (2006) Monthly Report on Earthquakes and Volcanoes in Japan November 2006. pp 37–45 (in Japanese). https://www.data.jma.go.jp/svd/eqev/data/gaikyo/monthly/200611/monthly200611.pdf

Japan Meteorological Agency (2010a) About the February 27, 2010 Maule Earthquake, JMA 2010 Press Release (in Japanese). https://www.jma.go.jp/jma/press/1003/09c/kaisetsu100309.pdf
Japan Meteorological Agency (2010b) Earthquake that occurred off the coast of central Chile at 15:34 on February 27, 2010 (5th report). JMA 2010 Press Release (in Japanese). https://www.jma.go.jp/jma/press/1003/01a/kaisetsu201003011000.pdf
Japan Meteorological Agency (2011) Monthly Report on Earthquakes ancd Volcanoes in Japan March 2011, 57–148 (in Japanese). https://www.data.jma.go.jp/svd/eqev/data/gaikyo/monthly/201103/monthly201103.pdf
Japan Meteorological Agency (2021) Performance verification of statistical tsunami attenuation prediction methods. Study Group on Tsunami Prediction Technology, 18th Meeting, Ref. 2-3 (in Japanese). https://www.data.jma.go.jp/svd/eqev/data/study-panel/tsunami/benkyokai18/shiryou2-3.pdf
Kajiura K (1963) The leading wave of a tsunami. Bulletin of Earthquake Research Institute. Univ Tokyo 41:535–571. https://doi.org/10.1016/0011-7471(65)90572-3
Koshimura S, Munemoto K, Oie T, Yanagisawa H, Abe I, Imamura F (2007) The effect of Emperor seamounts on the propagation of the 2006 Kuril Island tsunami. Proceedings of coastal engineering, JSCE, 54, I_171–I_175 (in Japanese with English abstract). https://doi.org/10.2208/proce1989.54.171
Matsumoto K, Takanezawa T, Ooe M (2000) Ocean tide models developed by assimilating TOPEX/POSEIDON altimeter data into hydrodynamical model. A Global Model and a Regional Model around Japan. J Oceanogr 56:567–581. https://doi.org/10.1023/A:1011157212596
Mori N, Takahashi K, The 2011 Tohoku earthquake tsunami joint survey group (2012) Nationwide post event survey and analysis of the 2011 Tohoku earthquake Tsunami. Coast Eng J 54(1):125000. https://doi.org/10.1142/S0578563412500015
Cabinet Office (2012) List of Maximum Tsunami Elevations by Prefecture and Municipality (High Tide Elevation). Publication of Tsunami Height, Inundation Area, and Damage Assumption for the Nankai Trough Giant Earthquake. https://www.bousai.go.jp/jishin/nankai/taisaku/pdf/1_2.pdf
Okada Y (1985) Surface deformation due to shear and tensile faults in a half space. Bull Seismol Soc Am 75(4):1135–1154. https://doi.org/10.1785/BSSA0750041135
Saito T, Inazu D, Tanaka S, Miyoshi T (2013) Tsunami coda across the pacific ocean following the 2011 Tohoku-Oki earthquake. Bull Seismol Soc Am 103(2B):1429–1443. https://doi.org/10.1785/0120120183
Satake K, Fujii Y, Harada T, Namegaya Y (2013) Time and space distribution of coseismic slip of the 2011 Tohoku earthquake as inferred from tsunami waveform data. Bull Seismol Soc Am 103(2B):1473–1492. https://doi.org/10.1785/0120120122
Tanioka Y, Satake K (1996) Tsunami generation by horizontal displacement of ocean bottom. Geophys Res Lett 23(8):861–864. https://doi.org/10.1029/96GL00736
Tanioka Y, Shibata M, Yamanaka Y, Gusman AR, Ioki K (2019) Generation mechanism of large later phases of the 2011 Tohoku-oki tsunami causing damages in Hakodate, Hokkaido, Japan. Prog Earth Planet Sci 6(1):30. https://doi.org/10.1186/s40645-019-0278-x
Yoshimoto M, Watada S, Fujii Y, Satake K (2016) Source estimate and tsunami forecast from far-field deep-ocean tsunami waveforms—The 27 February 2010 Mw 8.8 Maule earthquake. Geophys Res Lett 43:659–665. https://doi.org/10.1002/2015GL067181

Publisher's Note